Received: 23 January 2020 | Revised: 2 April 2020 | Accepted: 13 April 2020

DOI: 10.1002/ppap.202000016

FULL PAPER

PLASMA PROCESSES AND POLYMERS

An investigation on effectiveness of temperature treatment for fluorine-based reactive plasma jet machining of N-BK7®

Faezeh Kazemi[1] | **Georg Boehm**[1] | **Thomas Arnold**[1,2]

[1]Department of Precision Surfaces, Leibniz Institute of Surface Engineering (IOM), Leipzig, Germany

[2]Faculty of Mechanical Science and Engineering, Institute of Manufacturing Science and Engineering, Dresden, Germany

Correspondence
Faezeh Kazemi, Department of Precision Surfaces, Leibniz Institute of Surface Engineering (IOM), Permoserstraße 15, 04318 Leipzig, Germany.
Email: faezeh.kazemi@iom-leipzig.de

Funding information
German Federal Ministry of Education and Research (BMBF) within the framework of the InnoProfile-Transfer initiative, Grant/Award Number: 03IPT706X

Abstract

In this study, a fluorine-based reactive plasma jet is investigated as a promising tool for ultraprecise surface machining of N-BK7®. Plasma-generated particles react with an N-BK7 surface to create volatile and nonvolatile compounds. The desorption of volatile compounds results in an etched surface, whereas nonvolatile compounds form a residual layer in the etched area, causing unpredictable effects on the etching rate. Surface temperature treatment is proposed to improve the machining procedure with respect to deterministic material removal, leading to predictable results. It is shown that, at an elevated surface temperature, the residual layer properties are modified in favor of improved etching performance. The etching behavior of N-BK7 is compared with fused silica to verify the optimality of the obtained results.

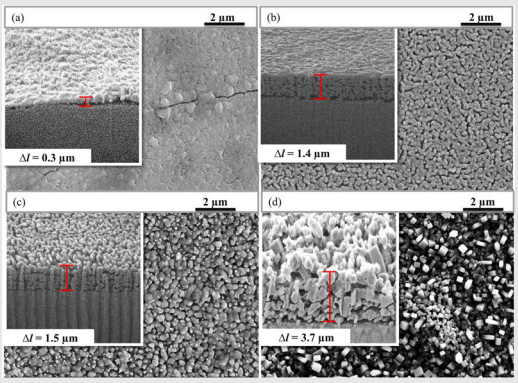

KEYWORDS
etching kinetics, fluorine, optics, plasma etching, surface modification

1 | INTRODUCTION

Plasma jet machining (PJM) is one of the well-known ultraprecision surface machining methods that employ a reactive plasma jet as a deterministic subaperture etching tool for the generation and correction of highly precise optical surfaces such as mirrors and freeform lenses.[1–3] Subaperture tools exhibit smaller lateral dimensions than the surface to be treated, and the surface can be scanned by these tools. Thus, the plasma jet as a subaperture tool allows high flexibility for machining of surfaces with complex shapes. As such, it is appropriate for the application in freeform optics manufacturing.[4] Moreover, PJM is a contactless technique in which the machining process relies on a purely chemical mechanism, converting the solid surface into gaseous compounds without any contributions of energetic ions and exerting practically no mechanical forces on the surface.[5] Therefore, no mechanical defects are introduced on the

surface during the process. Several authors have reported on successful fluorine plasma-based deterministic machining of fused silica, SiC, ULE®, or silicon for optical surface fabrication and freeform manufacturing, in particular.[6–8] However, as shown in our previous work, there are some limitations when this technique is used for surface machining of optical glasses containing components that cannot be converted into gaseous species like N-BK7®.[9,10] N-BK7 is a barium borosilicate glass known for its good optical properties and reasonable price, which can be an alternative for more expensive optical elements such as fused silica in an advanced optical industry.[11,12]

The chemical interaction between plasma-generated active species and metal components of N-BK7 induces the formation of a residual layer on the plasma–surface contact zone and surrounding, which can noticeably degrade the capability of acquiring a required surface profile for N-BK7 and lead to an irregular removal behavior. As shown in our previous work, the material removal rate decreases nonlinearly with the increase in the thickness of the residual layer.[9,10]

The aim of this study is to improve the N-BK7 surface machining by using fluorine-based reactive plasma jet in terms of deterministic material removal, leading to predictable results, which allows to go one step forward in the production of N-BK7 freeform optics. The surface temperature T_s is proposed here as a decisive factor for improving the performance of N-BK7 surface machining with respect to etching rate and surface quality. To demonstrate the effects of surface temperature, surface machining of N-BK7 is performed at different substrate temperatures. Subsequently, the chemical and structural characterization of the residual layer is analyzed by X-ray diffraction (XRD), X-ray photoelectron spectroscopy (XPS), and scanning electron microscopy (SEM). For more investigation, SEM analysis is incorporated with a focused ion beam (FIB) preparation and energy-dispersive X-ray spectroscopy (EDX). By analyzing the experimental results, it is revealed that the surface temperature has strong effects on the thickness and morphology of the residual layer that forms during the etching process. Moreover, the machining performance of N-BK7 is compared with that of fused silica to verify the optimality of the obtained results.

Finally, a dynamic machining process is performed at elevated surface temperatures. It is demonstrated that unfavorable effects of the residual layer on surface machining of N-BK7 are suppressed, and the local etching rate is enhanced at high surface temperatures. Therefore, improved results in terms of etch homogeneity and predictability are obtained for surface machining.

2 | EXPERIMENTS

2.1 | Experimental setup

All experiments in this study are performed in a vacuum chamber, which is equipped with a plasma jet source, a three-axis motion system, a substrate heater, and an infrared thermography camera (Optris PI 160; see Figure 1). The substrates are placed on a heater that can be moved in the *x*- and *y*-direction, respectively. The plasma jet source, which consists of a set of two concentrically arranged nozzles (shown in Figure 1), is mounted on the *z*-axis of the motion system. Mass flow controllers (Bronkhorst EL-FLOW) are used to adjust the gas feed rates of the plasma jet source. The inner nozzle is fed by 400 sccm He as an inert carrier gas and 1 sccm CF_4 as a reactive plasma component.

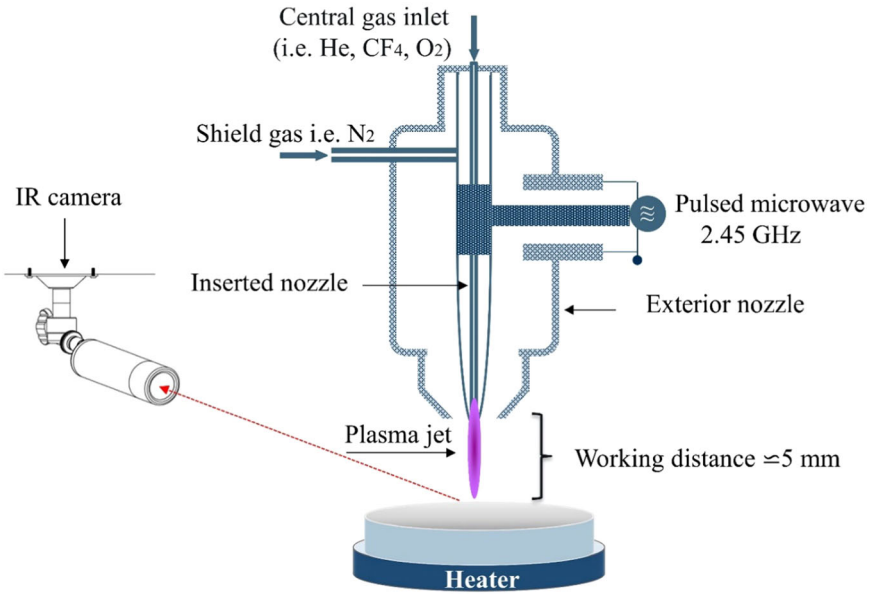

FIGURE 1 Schematic drawing of the reactive plasma jet interacting with the N-BK7® surface during the PJM process. IR, infrared; PJM, plasma jet machining

According to our last investigation, the addition of a sufficient amount of O_2 impedes fluorocarbon film deposition and increases the etch rate in CF_4 plasmas.[9] Hence, a certain amount of O_2, depending on the material that is etched (i.e., 1 sccm for fused silica and 2 sccm for N-BK7), is admixed to CF_4 in all experiments. As an inert shielding gas, 400 sccm N_2 is provided through the outer nozzle to stabilize the plasma jet discharge. The gas feeding nozzles are made of metal; hence, they act as inner and outer electrical conductors of a coaxial line to conduct the microwave excitation energy. A custom-made solid-state generator provides microwave power at 2.45 GHz and a pulse generator is employed to produce a pulsed microwave signal. Microwave power is coupled to the plasma jet source in the form of rectangular pulses. Effective microwave power is measured by a directional power sensor (Rhode & Schwarz NRT-Z44) located between the generator and the plasma source. The maximum electric field intensity arises around the tip of the inner nozzle where the plasma is ignited. The mean input power P_M of plasma jet can be calculated in units of W according to the following:

$$P_M = t_p \times P_p \times f_p, \quad (1)$$

where f_p denotes the pulse repetition frequency in kHz, P_p is the pulse peak power in W, and t_p is the pulse width in μs. For all experiments, a repetition frequency of 2.1 kHz is adjusted, whereas the peak power and the pulse width are, respectively, set as 200 W and 38 μs, resulting in a mean power of approximately 16 W. The working distance between the nozzle and sample during the etching process is set as 5 mm.

For the investigation of the etching mechanism, three simple motion schemes performed by the three-axis system are applied. (a) For static etching, the plasma jet is placed perpendicular to the substrate surface to generate a footprint pattern. Depending on the etching time t, a certain etching depth profile D is created. (b) For dynamic etching, the plasma jet is moved along one-axis motion. In this case, a line pattern is obtained when the plasma jet repeatedly moves on a linear path over the surface with a fixed velocity v. (c) A rectangular area is etched by moving the plasma jet in a raster path mode at a constant velocity and a line feed Δy.

Before starting a surface machining process, the chamber is evacuated to a minimum pressure of 0.5 mbar using a rotary slide and roots pumps. Subsequently, the chamber pressure during the experiments is fixed to 900 mbar via the inlet of N_2 and with the aid of a pressure-controlled throttle valve located in the exhaust pipe.

2.2 | Specimen preparation

The etching process was performed on optically polished N-BK7 wedged windows and fused silica windows (supplied by Edmund Optics) with a thickness of 3 mm and diameter of 50 mm. A typical feature of N-BK7, compared with fused silica glass (99.93% silica), is the presence of about 20% of boron trioxide and alkaline oxide in its chemical composition, which affects its properties. The nominal composition of N-BK7 is given as follows: 57.9% O, 25.4% Si, 4.7% C, 3.9% Na, 3.5% B, 3.2% K, 0.5% Ca, 0.4% Mg, 0.3% N, 0.2% Zn, and 0.1% Ba.[13]

Before performing the etching process, all specimens were treated in an ultrasonic cleaning bath for 30 minutes at 50°C by a solution of 1-ml NH_4OH, 2-ml H_2O_2, and 40-ml H_2O, and then by a solution of 1-ml HCl, 2-ml H_2O_2, and 8-ml H_2O for another 30 min at 50°C. For the case of N-BK7, the residual byproducts that form on the surface during plasma processing have to be removed to ensure a precise depth profile measurement by an optical surface profiler on the etched surfaces. It was found in our previous work that most of these residual products are soluble in a water/ethanol solution.[9] Thus, after the process, the N-BK7 specimens are cleaned with 1:1 water/ethanol solution before cleaning with the above-mentioned solutions.

2.3 | Surface temperature measurement

Substrate surface temperature distributions were measured by an infrared (IR) thermography camera (Optris PI 160), which is capable of acquiring temperatures in a range between 0°C and 550°C. The calibration of the emissivity for the surface temperature measurements on polished N-BK7 was performed on the basis of the comparison of the surface temperature of a black sooth layer ($\varepsilon = 0.98$) partly applied on the N-BK7 substrate and the temperature of the bare glass surface; however, the substrate was externally heated to several temperature levels. The emissivity of polished N-BK7 was determined to be $\varepsilon_{N-BK7} = 0.7$.

The IR camera was located at a fixed position, focusing on the substrate surface. Thus, the temporal temperature curves and local temperature distributions are referred to the plasma jet center point. The local surface temperature T_s during the surface machining increases with the plasma heat flow, as the plasma jet acts as a significant heat source on the substrate surface. Depending on the plasma mean input power, dwell time, and thermal coupling of the substrate with the environment, a characteristic spatiotemporal temperature distribution develops during the etching process. It should be noted that the transition temperature T_g of N-BK7 is 550°C.[14]

Thus, during the machining process, the surface temperature T_s was controlled to ensure that it was well below T_g.

2.4 | Surface analysis

A white light interferometer (WLI) microscope (Bruker NPFLEX) was used throughout this study for the determination of cross-section profiles of etched structures on the substrate surface, where 10 parallel depth profiles were averaged for every structure. Microroughness was measured by WLI microscope using ×50 objective, and X-ray photoelectron spectroscopy (XPS; Instrument Axis Ultra DLD; KRATOS, Manchester, UK) was used to determine the chemical composition of the surface. Moreover, the surface composition mapping was performed by scanning electron microscopy–energy-dispersive X-ray (SEM–EDX) measurements in a Zeiss Gemini Ultra 55 machine with a Bruker XFlash 3001 detector. FIB was employed to prepare vertical cross-sections through residual layers that have been subsequently analyzed by SEM.

3 | ETCH MECHANISMS FOR DIFFERENT SURFACE TEMPERATURES

The aim of the current investigations is to clarify the underlying mechanisms of material removal, layer formation, and surface roughness evolution on N-BK7 surfaces during plasma jet etching at varying surface temperature. With the understanding gained and by determination of the spatiotemporal distribution functions of material removal (also referred to as tool function) for different process conditions, a database is obtained, which can further be used for simulation of dynamic etching processes in the framework of a deterministic surface figuring process. In our assessment framework, the results for fused silica are presented for comparison, as the surface machining of fused silica by plasma jet is well established.

As PJM is a pure chemical machining process, the etching rate R at a given surface temperature T_s can be expressed by the Arrhenius equation:

$$R = A\mathrm{e}^{-\frac{E_a}{k_B T_s}}, \tag{2}$$

where k_B denotes the Boltzmann constant, A is the pre-exponential factor, and E_a is the activation energy.[15]

In the case of fused silica, the chemical reactions of plasma-generated active fluorine atoms with fused silica (SiO_2), which exclusively form volatile etching products SiF_4 and CO_2, are used to obtain the local material removal on the substrate. According to the Arrhenius equation (2), the variation of surface temperature can slightly change the etching rate of fused silica. Compared with fused silica, the chemical interaction of N-BK7 surface with the fluorine-based plasma discharge is more complex and much more affected by the variation of surface temperature. As PJM of N-BK7 employing plasma jet is a pure chemical process, one can expect that temperature T_s has a major effect on the chemical kinetics of the substrate surface and consequently on the local etching rate.[15]

As it was mentioned earlier,[13] roughly 80% of the nominal composition of N-BK7 contains silicon, oxygen, and boron, which together constitute the N-BK7 glass network formers (i.e., silica [SiO_2] and boron trioxide [B_2O_3]). Hence, the chemical interactions of these elements with the fluorine-based plasma discharges produce exclusively volatile products, SiF_4 (g), CO (g), CO_2 (g), BF_3 (g), B_2F_4 (g), and COF_2, and the desorption of these volatile products yields the etched surface.[9] The increase in the surface temperature leads to higher chemical reaction rates and accelerates the desorption rate of volatile etched products. Thus, the attainable material removal is noticeably affected by the temperature. However, about 20% of the N-BK7 nominal composition consists of metal elements (i.e., barium, potassium, and sodium). The reactions between the fluorine-based plasma discharge and metal elements proceed spontaneously in a kinetically favorable way to produce nonvolatile fluorine–metal compounds such as NaF(s), KF(s), and BaF_2. As these products have a very high boiling point, they are solid under normal conditions and cannot desorb from the surface. Hence, they create a residual layer on the N-BK7-etched area and surrounding.

In the following, the influence of temperature on the mechanisms of surface treatment for both fused silica and N-BK7 is evaluated by applying different temperatures to the surface at defined process parameters.

3.1 | Influence of plasma jet heat flux on surface temperature

To investigate the effects of surface temperature on the etching mechanism, the substrate was heated by a heater to initial temperatures T_h between 25°C and 350°C; however, all other process parameters were kept fixed. The final value of surface temperature T_s is obtained by the sum of the plasma heat flow and the heat flow originating from the heater. The influence of plasma-induced heating was determined for static etchings at different initial temperatures T_h. Figure 2 shows snapshots of the lateral surface temperature distribution

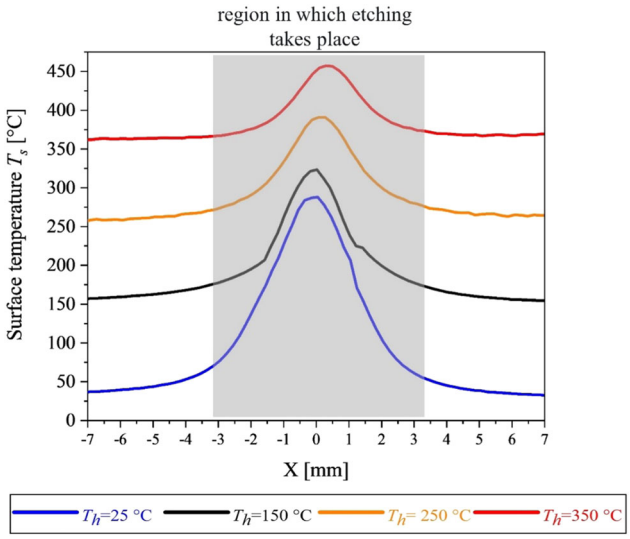

FIGURE 2 Snapshots of lateral surface temperature distributions during static etching obtained for four different initial temperatures T_h: 25°C, 150°C, 250°C, and 350°C at plasma etching time $t = 8$ s

perpendicular to the plasma jet for initial temperatures $T_h = 25$°C, 150°C, 250°C, and 350°C during static etching with a plasma etching time $t = 8$ s. As it is illustrated in Figure 2, when the plasma affects the surface, a sudden rise of temperature is observed. Due to the extra heat of the plasma flow, the maximum surface temperature T_s is observed at the center of the plasma jet–surface interaction zone, and it reaches 280 ± 10°C, 310 ± 10°C, 380 ± 10°C, and 470 ± 10°C for the four different initial temperatures T_h, respectively. It can be observed that the lateral distribution of surface temperature T_s has a nearly Gaussian shape. It approaches gradually to the initial surface temperature T_h at the peripheral area of the plasma interaction zone. In case of a lower initial temperature (e.g., $T_h = 25$°C), the impact of plasma heat flux on the surface temperature T_s becomes greater and provides a larger heat transfer to the surface. Therefore, a higher initial temperature T_h helps to adopt a more uniform surface temperature T_s over the radial profile during the process and, to some extent, inhibits the sudden rise of surface temperature T_s at the beginning of etching.

However, it should be noted that when the surface temperature T_s is higher than the transition temperature T_g of N-BK7, the effect of temperature is not any more conducive to form a smooth surface. It rather introduces damage to the surface. Therefore, it is necessary to strictly control the surface temperature during the machining process to ensure that the temperature is below T_g. In our case, the optimal surface temperature $T_s = 480$°C is still below the transition temperature $T_g = 550$°C.[14]

3.2 | Effect of surface temperature on material removal

In this section, footprint patterns were generated on the N-BK7 surface by using a static machining process at different surface temperatures T_s to obtain knowledge concerning the lateral distribution of residuals and the behavior of the local interaction of the plasma jet with the surface. Moreover, the etching performance of N-BK7 was evaluated, and the results were compared with fused silica. For this purpose, the cross-sectional profile and roughness of footprint patterns of N-BK7 at different initial temperatures T_h were determined after the residual layers were removed by water/ethanol solution. Figure 3 presents the effect of surface temperature T_s on the temporal evolution of etch profile depth for N-BK7. In this regard, the cross-sections for different etching times t (1, 2, 4, 6, 8, 10, and 12 s) are shown for different initial surface temperatures T_h.

As surface machining of fused silica by plasma jets is well understood, the results for fused silica are also provided in Figure 4 for comparison when the surface is not preheated (i.e., $T_h = 25$°C); however, all other conditions are kept the same. In this case, the material removal is obtained by the chemical reactions of fluorine and oxygen with the fused silica surface, forming an exclusively volatile etching product, that is, SiF_4. The resulting etch profile exhibits a near-Gaussian functional form, where the maximum etching depth (in a simple approximation disregarding temperature changes during footprint etching) is a linear function of etching time *t*.

As it was presented and discussed in our previous work, the radial depth profiles on N-BK7 surfaces generated by static footprint etchings at $T_h = 25$°C exhibit a much more complex structure, depending on etching time, compared with fused silica.[9]

It can be observed from Figure 3a that for short etching times (i.e., $t \leq 2$ s), the shape of etch profile is near-Gaussian, similar to fused silica (see Figure 4). In this case, the N-BK7 etch profile is not significantly hindered by the residual layer, as it is too thin; hence, an expected distribution of reactive particle densities on the surface is achieved, which leads to isotropic etching. The temporal behavior of the profiles shown in Figure 3a for $t > 2$ s is mainly attributed to the formation of an alkali fluoride layer, inhibiting the etching process in the center part, whereas the tangential process gas transport phenomena lead to a removal of the layer at a radius of approximately 0.8 mm, spreading the material in the surrounding. For larger etching times ($t > 2$ s) and low initial temperatures $T_h < 150$°C, the etch profiles deviate significantly from the Gaussian distribution, leading to a flattened profile shape. By further increasing the etching time *t*, material removal

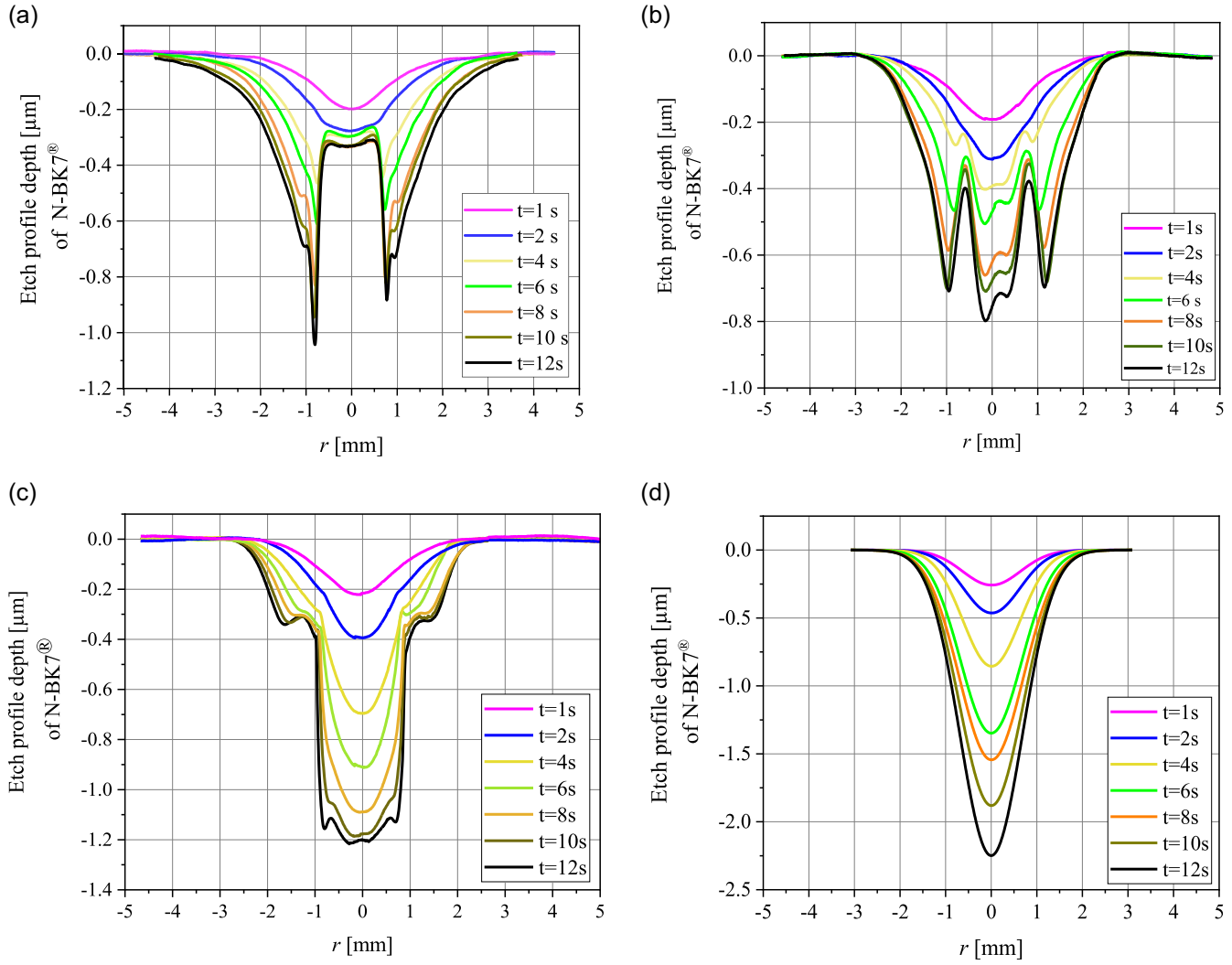

FIGURE 3 Temporal evolution of N-BK7 etch profiles during static plasma processing at different initial temperatures T_h: (a) 25°C, (b) 150°C, (c) 250°C, and (d) 350°C after the removal of the residual layer with water/ethanol

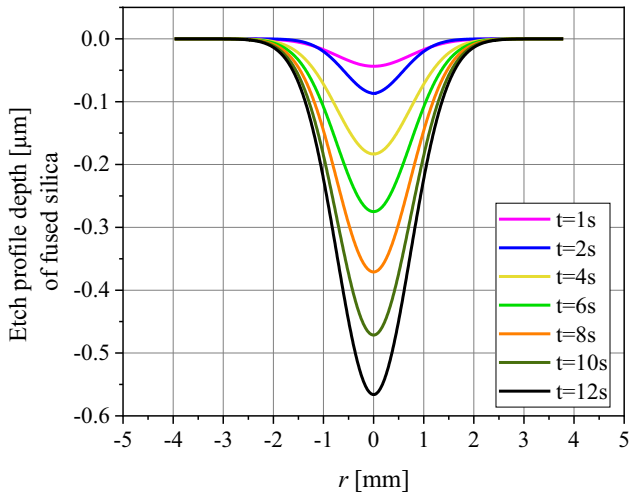

FIGURE 4 Etch profile depth obtained by the reactive plasma jet on the unpreheated surface of fused silica after static plasma processing

is barely observed at the center, whereas a sharp etching structure is achieved at the peripheral area (see Figure 3a). Apparently, at the center, the residual compounds accumulate and mask the surface underneath by obstructing the diffusion of fluorine atoms into the surface of N-BK7. Eventually, the endpoint of etching occurs at a etching time $t = 12$ s, where the residual layer completely prevents the attack of etching species even at the peripheral area (see Figure 3a). One can observe from Figure 3b,c that by increasing the initial temperature T_h, the flattened (non-Gaussian) shape of the etch profiles at large etching times ($t > 2$ s) gradually changes to a more Gaussian-like profile. Obviously, at the center, the residual compounds do not mask the surface underneath to impede the continuous and isotropic etching. Finally, when the surface is adequately preheated, $T_h = 350$°C, the etch profiles have a near-Gaussian shape, indicating isotropic etching even for larger values of the etching time t (see Figure 3d).

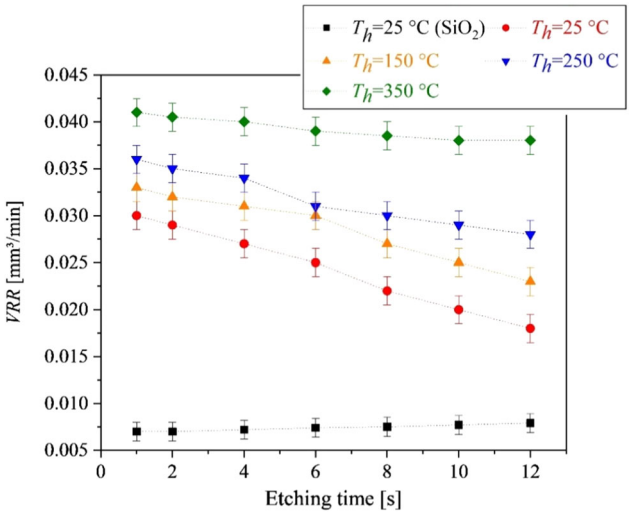

FIGURE 5 Time-dependent volumetric removal rates (VRR) obtained for different surface temperatures T_s

The volumetric removal rate (VRR) for the footprint pattern is calculated in terms of the local etching depth $D(r)$ and the etching time t as follows:

$$\mathrm{VRR} = \frac{1}{t}\int_{-r_{\max}}^{r_{\max}} D(r)\ 2\pi r\, dr, \tag{3}$$

where $r_{\max}$ is the maximum distance from the center of the radial profile. The etch profile depths presented in Figures 3 and 4 are used for computing VRR at different conditions with respect to etching time t by Equation (3), and the obtained results are shown in Figure 5. One can observe from this figure that VRR for fused silica is roughly linear with respect to the etching time t, whereas VRR for N-BK7 is a decaying nonlinear function of etching time t that exhibits a rather irregular behavior. However, by increasing the initial temperature to $T_h = 350°C$, the VRR becomes more predictable, exhibiting a stable behavior that could be described by an exponential decay law.

3.3 | Analysis of residual layers on N-BK7 surface, depending on the surface temperature

It was shown that by applying a certain etching time t, a residual layer forms on the N-BK7 surface, exhibiting inhomogeneous thickness distributions, which consequently leads to a complex-shaped lateral surface profile and strongly nonlinear material removal.[9] Although the thickness evolution of the residual layer by an increase of etching time t is inevitable, its characteristics during the machining process were modified by adjusting the surface temperature T_s. Hence, the surface temperature T_s is a significant factor that affects not only the N-BK7 etching rate but also the features of the formed residual layer in the etching zone such as thickness and structure. In this section, to determine the impact of the surface temperature T_s on the properties of the residual layer, the N-BK7 surface was preheated to initial surface temperatures $T_h \in 25°C$, 150°C, 250°C, and 350°C. Dynamic and static machining processes were performed for varying etching times t, in which a significantly thick residual layer was expected.

3.3.1 | Lateral distribution of residual layer

Figure 6 illustrates EDX images of the distribution of residual compounds over the radial profile r for footprint patterns at different initial temperatures T_h and static etching time $t = 8$ s. In this figure, the main components of the substrate (Si and O) and the residuals (Na, K, and F) are color-coded. It can be observed that at each specific surface temperature, the lateral distribution of the residual layer exhibits its own characteristic pattern.

As it is observed in Figures 3a and 6a, during etching, a masking layer is formed, which strongly hinders continuous etching. However, the layer appears cracked in clods. In the periphery at $r = 800\ \mu m$ approximately, the residual layer is delaminated in a ring-shaped zone, whereas for a larger radius, a closed layer with decreasing thickness is visible. When the surface is not preheated (i.e., the initial temperature $T_h = 25°C$), the local surface temperature T_s at the center of the footprint reaches 280°C. It deviates largely from that of the peripheral area due to the plasma heat flow (i.e., Figure 2a). Cracking and delamination are, thus, attributed to the relatively high temperature gradient over the radial profile, leading to thermal stress in the layer. Layer removal in the ring-shaped zone may be due to the lateral gas flow that shows a maximum tangential velocity at $r = 800\ \mu m$, as it was discussed in our previous study.[9]

In the case that the sample is preheated to the initial temperature $T_h = 150°C$ (see Figure 6b), the radial distribution of residual layer exhibits a similar structure, compared with the latter case, except that the central part is delaminated. Only some of clod-like portions remain in this region. As it is conceived from the etch profiles in Figure 3b, the etching depth at the center is 0.8 μm (compared with 0.3 μm in the non-preheated case), suffering from a higher accumulation of residues locally. Hence, under this circumstance, a higher thermal stress is induced in the residual layer, leading to cracking and layer removal. If preheating temperature T_h is increased to 250°C, a

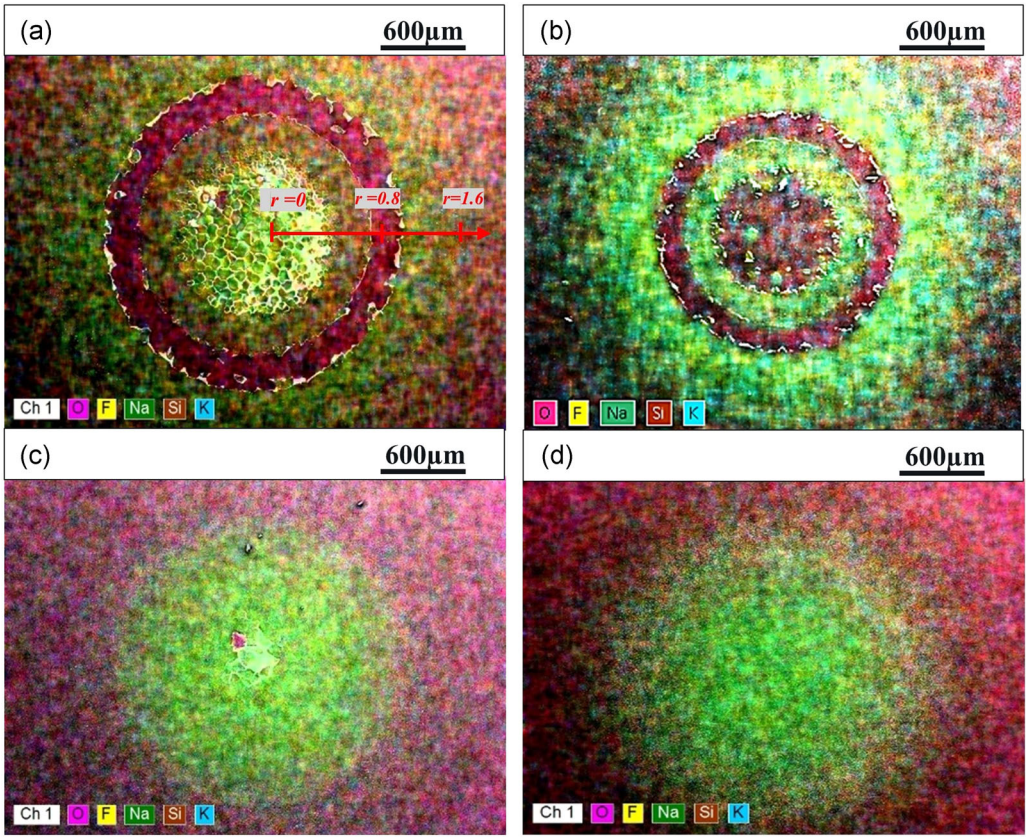

FIGURE 6 Energy-dispersive X-ray spectroscopy images of the footprint obtained after static etching for etching time $t = 8$ s at different initial temperatures T_h: (a) 25°C, (b) 150°C, (c) 250°C, and (d) 350°C

uniformly closed residual layer is formed, and only a marginal delamination occurs in the center, which is not visible at all for $T_h = 350$°C (see Figure 6c,d).

3.3.2 | Morphology of the residual layer

The resulting surface morphology and thickness of residuals formed on the N-BK7 surface after a plasma area scanning treatment were analyzed at a constant velocity of 2 mm/s, line feed Δy of 0.1 mm, and different surface temperatures T_s. FIB vertical cross-sections were prepared and imaged by SEM. Furthermore, the SEM images in the top-view configuration were obtained. The results are illustrated in Figure 7. For $T_h = 25$°C/$T_s = 280$°C, a layer of approximately 0.3-µm thickness is created, exhibiting a granular but densely packed structure. Eventually, some cracks are observed (Figure 7a). At $T_h = 150$°C/$T_s = 310$°C, the layer is 1.4-µm thick and shows evenly distributed pores or voids in the cross-section. The top view reveals smaller granules that are less-densely packed and the voids are visible as well (Figure 7b).

If the surface is heated to $T_h = 250$°C/$T_s = 380$°C, the layer thickness increases to 1.5 µm. There is an increase in voids as well as the size of the granules, which resemble a partly crystalline structure with regular edges (Figure 7c). For the highest temperature applied ($T_h = 350$°C/$T_s = 470$°C), the layer shows a thickness of 3.7 µm; large pores are visible in the cross-section and the crystalline structure of the granules is obvious. (Figure 7d). The findings are discussed as follows:

When the N-BK7 surface is not preheated, a sudden rise of temperature is imposed locally into the contact area of the plasma-treated zone by applying plasma heat flow. Therefore, this noticeable variation of surface temperature T_s during area etching in the plasma-contact zone and surrounding causes a thermal shock to the nonvolatile compounds. Hence, the residuals rearrange into a less ordered form, accumulate, and create a closely compact layer. Although the formed residual layer is thin, it is dense enough to mask the surface underneath and obstruct the diffusion of fluorine atoms through the layers into the surface of N-BK7.

However, by preheating the sample gradually, the surface becomes less likely to be subjected to an abrupt rise of temperature imposed by the plasma heat flow and the thermal gradient seen by the surface is reduced. Therefore, the residual compounds formed during the

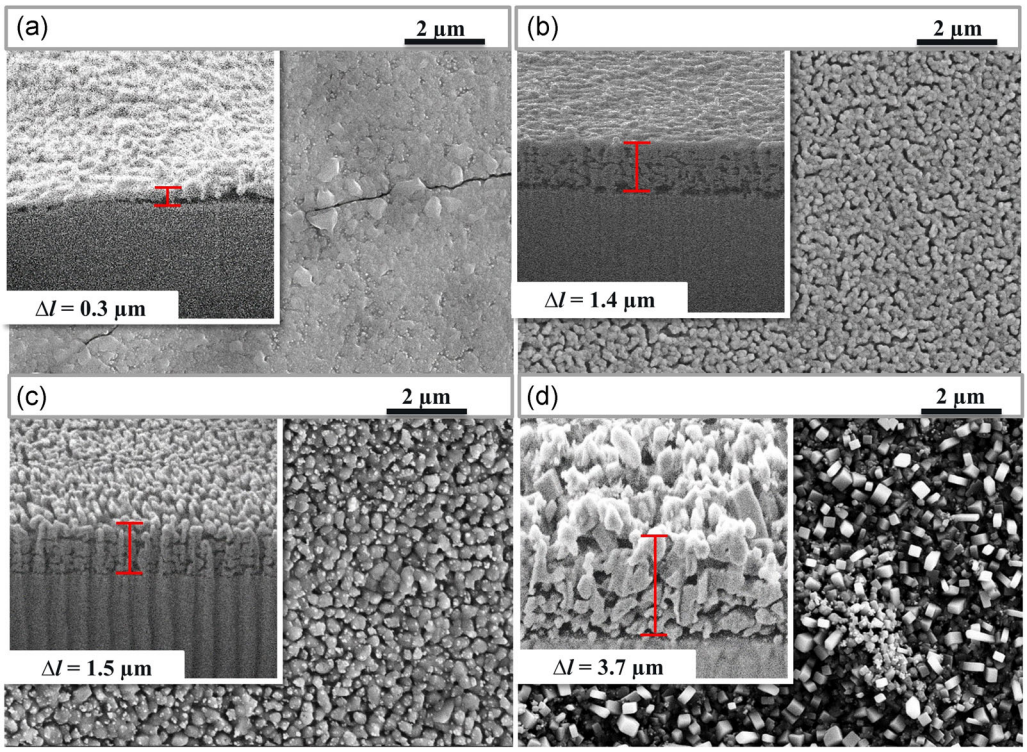

FIGURE 7 Surface morphology SEM of N-BK7 after area etching at four different initial temperatures T_h: (a) 25°C, (b) 150°C, (c) 250°C, and (d) 350°C by preheating the sample. The measured layer thickness is denoted in the plots by Δl

machining process remain for a longer time at high temperature. They solidify gradually; consequently, they can rearrange into a more ordered crystalline form. As shown in Figure 7d, such ordered crystallites that build up at a high surface temperature T_s have more cavities that allow the diffusion of fluorine atoms through the layers into the N-BK7 surface. Therefore, etching proceeds for much larger values of etching time t, and a much thicker layer forms on the surface.

To prove the crystallinity of the residual layer, XRD measurements were performed, and the spectra are presented in Figure 8. The results show that for the lowest temperature, there is an occurrence of a broad band, which is identical to the spectrum obtained from an untreated N-BK7 reference sample. At increased surface temperatures, a growing number of narrow peaks appear in the XRD signals, which have maximum intensity for the highest surface temperature, indicating that the residual compounds solidify into a more crystalline form.

3.3.3 | XPS analysis of N-BK7 surface after area treatment

The four different plasma-treated areas, presented in Figure 7, were further analyzed by XPS to reveal the dependence of the chemical composition of the formed residual layer on the surface temperature T_s. The chemical composition of the unprocessed surface of N-BK7 is additionally measured as a reference. The results are depicted in Figure 9, which shows a wide variety of chemical elements belonging to either the N-BK7 glass components (e.g., Si, O, K, and Na) or plasma-generated reactants (F). By comparing the results, it can be observed that the arrangement, type, and ratio of atoms in the structure of the residual layer vary when there is a change in the initial temperature T_h. XPS spectra were analyzed and the relative abundance, in at%, was calculated. In the case of an initial temperature $T_h = 25°C$, the chemical composition of the residual layer shows a large amount of fluorine–metal compounds such as KF, NaF, BaF_2, $NaBF_4$, and Na_2SiF_6. Moreover, low amounts of oxygen and silicon are measured in the composition. However, by increasing the initial temperature from $T_h = 25°C$ up to $T_h = 250°C$, the quantities of oxygen and silicon increase, whereas the quantities of fluorine, sodium, and potassium decrease.

Finally, once the sample is preheated, that is, the initial temperature $T_h = 350°C$, the chemical composition of the residual layer is dominated by oxygen and silicon. Although signals indicating fluorine, sodium, and potassium are detected, their intensity is still much less than that for lower initial temperatures, that is, for $T_h < 350°C$. This finding seems to be contrary to the

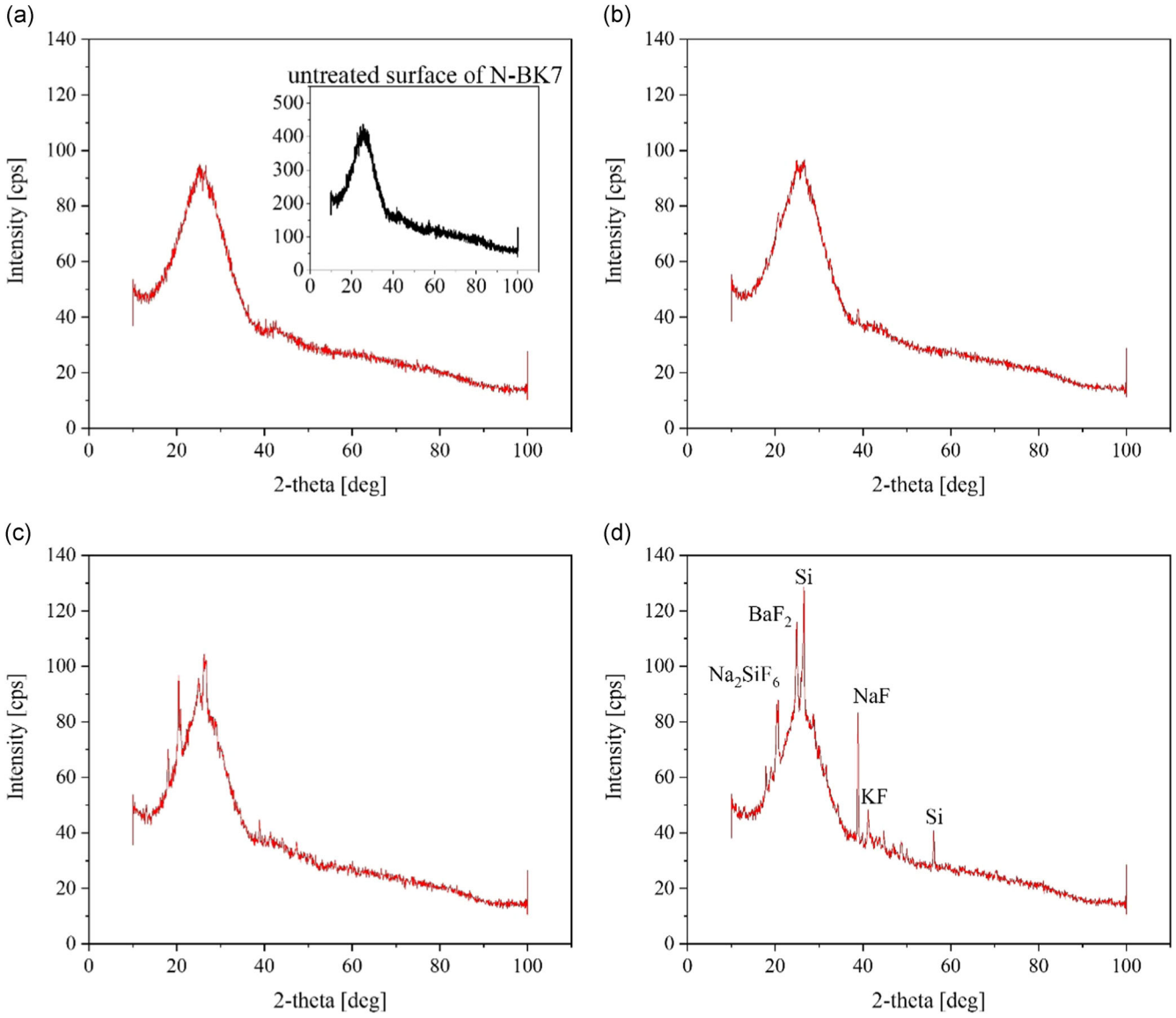

FIGURE 8 X-ray diffraction analysis of N-BK7® after area etching at four different initial temperatures T_h: (a) 25°C, (b) 150°C, (c) 250°C, and (d) 350°C by preheating the sample

results obtained from EDX, where the fluorine abundance is increased and the oxygen abundance is decreased for an increased temperature. However, information depth of EDX is in the micrometer range, whereas for XPS, the measurement signals arise from the topmost 10 nm, approximately. This would indicate that under high temperature conditions, a significant amount of SiO_2 is present on the layer surface; however, the layer itself consists mainly of alkali fluoride compounds. The presence of SiO_2 on the surface layer could be explained by the conversion of SiF_4 generated during the etching process and it might be still present in the pores and voids of the layer even after stopping the etching process. As the sample is brought to atmospheric environment after the plasma process, it comes into the contact with humidity, leading to hydrolysis of SiF_4, forming a thin film of SiO_2 on top of the granules.

3.3.4 | Surface roughness measurements

As the purpose of plasma jet machining technique is to process optical elements, the surface roughness evolution during the etching is of great interest. Figure 10 illustrates the influence of initial temperature T_h on the variation of N-BK7 surface roughness (per Sq) over the radial profile r that was etched with different values of etching time t. Before roughness measurement by WLI

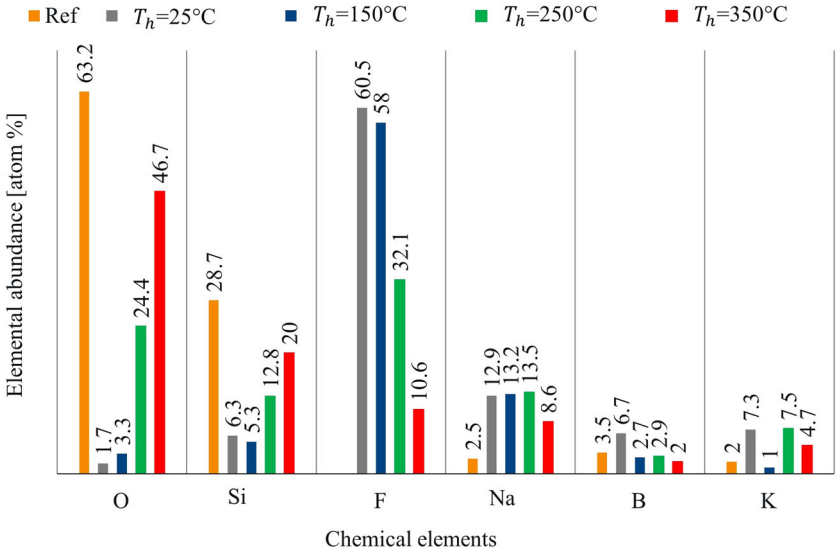

FIGURE 9 Chemical composition of the N-BK7 surface measured by X-ray photoelectron spectroscopy after the area etching at four different initial temperatures T_h: 25°C, 150°C, 250°C, and 350°C

technique, the surfaces were cleaned using the procedure described in Section 2.2. When the etching time t is less than 2 s, the etching for all initial temperatures T_h results in a relatively smooth surface, and the measured roughness of the footprint is Sq = 4 nm (see Figure 10, the curve at $t = 1$ s). However, by increasing the etching time t, the effect of initial temperature T_h on the surface roughness becomes more evident. When the surface is not preheated (i.e., Figure 10a) and the etching time t is large, the measured roughness over the radial profile r increases sharply, especially at the center of the etched footprint, reaching Sq = 70 nm. This roughness distribution can be attributed to the formation of multiple cracks and clods in the relatively dense layer, which is observed in Figure 6a. This layer acts as a non-uniform roughness mask, spatially modulating the attack of the underlying N-BK7 surface by the fluorine atoms. As the initial temperature T_h is increased to 150°C, the radial zone of high roughness broadens, which may be attributed to an extended zone of the cracked residual layer. At T_h = 250°C, the central part shows a significantly lower roughness of maximum Sq = 30 nm, whereas in the periphery, the roughness reaches Sq = 80 nm. It is shown in Figure 7 that for sufficiently high surface temperatures T_s, the residual layer shows a closed, noncracked but porous structure, allowing a more uniform etching attack. However, in the periphery, the layer seems to be denser but cracked, indicating that at this location, the surface temperature is not high enough to form a closed layer. Consequently, the roughness is higher at this location. If the initial temperature T_h is adjusted to 350°C, the increase of surface roughness is minimum, and a homogeneous distribution is observed. Obviously, the residual layer exhibits uniform properties determined by a surface temperature high enough to form a porous layer that can be penetrated by fluorine atoms to etch the underlying N-BK7 surface.

3.3.5 | Area etching at high surface temperature

It was shown in the previous sections that during static footprint etching, there is an occurrence of characteristic etching profiles, depending on the surface temperatures T_s, which show a high degree of complexity. However, it was observed that by increasing the surface temperature T_s through preheating the sample to 350°C, the influence of an inhomogeneous structured residual layer on the N-BK7 etch profile was suppressed. Hence, a uniform material removal with a comparably low surface roughness can be achieved over the radial profile. In this case, the etching rate follows a Gaussian function. Therefore, an initial temperature T_h = 350°C was chosen to perform a surface machining to assess the predictability of dynamic etching. Predictable dynamic etching is a prerequisite for a deterministic dwell time-based machining scheme. In the experimental setup, a raster path mode was employed with a constant line feed $\Delta y = 0.1$ mm, and the velocity v was stepwise increased after every 25 lines, starting from 1 to 12 mm/s (see Figure 11a).

During the dynamic machining process, the relative motion of the plasma jet leads to the convolution of the etching rate function R with the plasma dwell time (or equivalently the velocity of the plasma jet) at certain coordinates x and y. As the etching rate function R has a symmetric Gaussian shape at an elevated surface temperature (i.e., T_h = 350°C), the result of surface machining

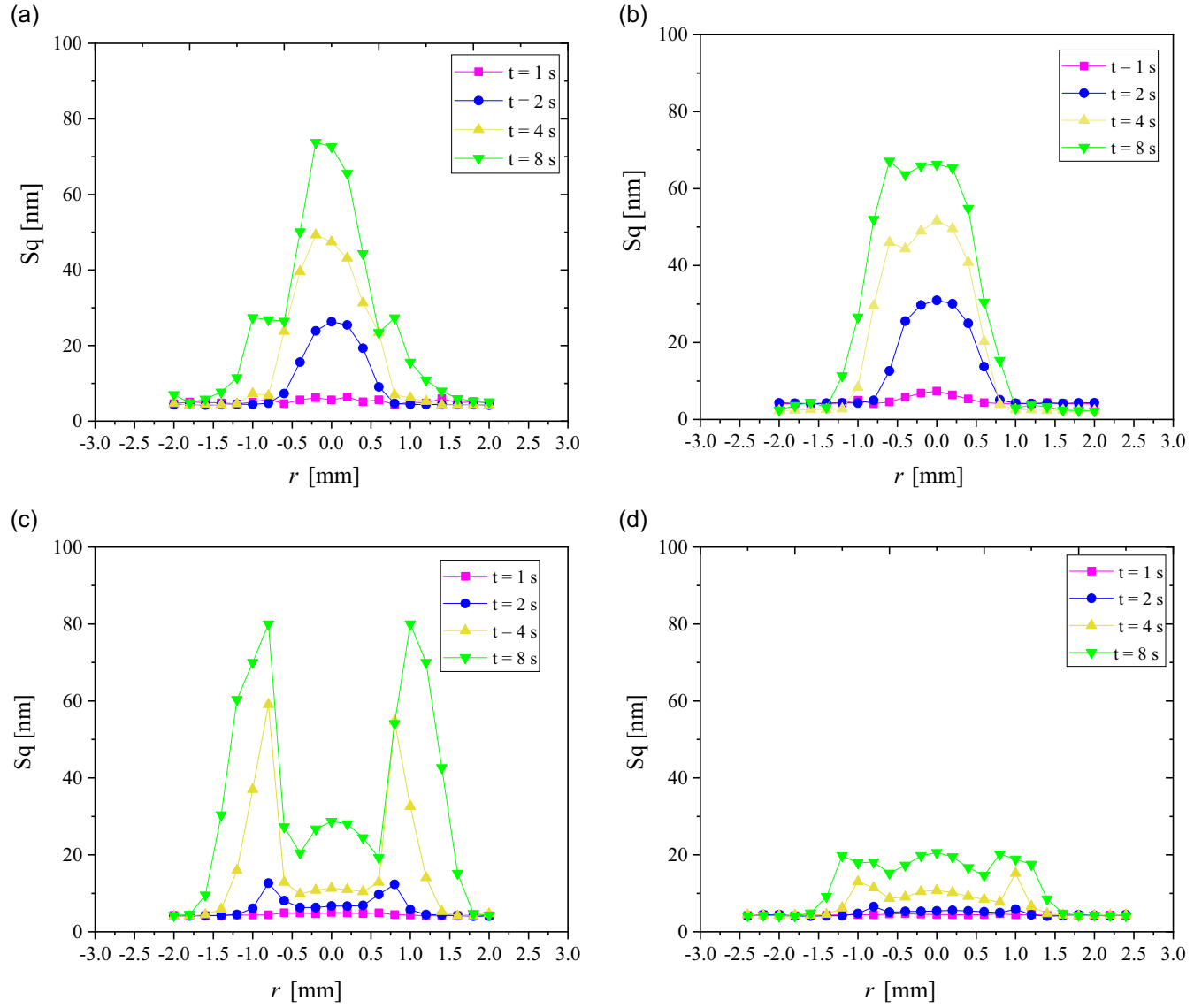

FIGURE 10 Surface roughness of N-BK7 after static etching at different etching times t over the radial profile r at various initial temperatures T_h: (a) 25°C, (b) 150°C, (c) 250°C, and (d) 350°C after the removal of residual layer with water/ethanol

provides a uniform etching profile h, which is predictable for different plasma dwell times (or equivalently different velocities of the plasma jet v). However, even at an elevated surface temperature, the etching rate decreases with the increase in the plasma dwell time due to the continuous growth of the residual layer. To show the effect of the residual layer on the reduction of etching rate, the VRR for area etching presented in Figure 11d, which is computed as follows:

$$\mathrm{VRR} = vh\Delta y. \tag{4}$$

One can observe from this figure that VRR strictly increases with velocity v. Furthermore, the surface roughness Sq over the radial profile is presented in Figure 11c; however, the velocity increases from $v = 1$ m/s to $v = 12$ mm/s. It can be observed from this figure that by increasing the velocity v, there is a decrease in the surface roughness. This finding corresponds to the previously discussed effects for high surface temperatures. By performing a deep etching, a residual layer with a thickness proportional to the measured etching depth is formed. Although this layer can be penetrated by fluorine atoms through its pores and voids, it reduces the removal rate and causes a relatively high surface roughness. With the decrease in the total etching depth, there is an increase in the VRR, whereas there is a decrease in the surface roughness.

The functional form of etching depth depends on the VRR and it should be taken into account if a deterministic machining process is performed. This task is subject to future work.

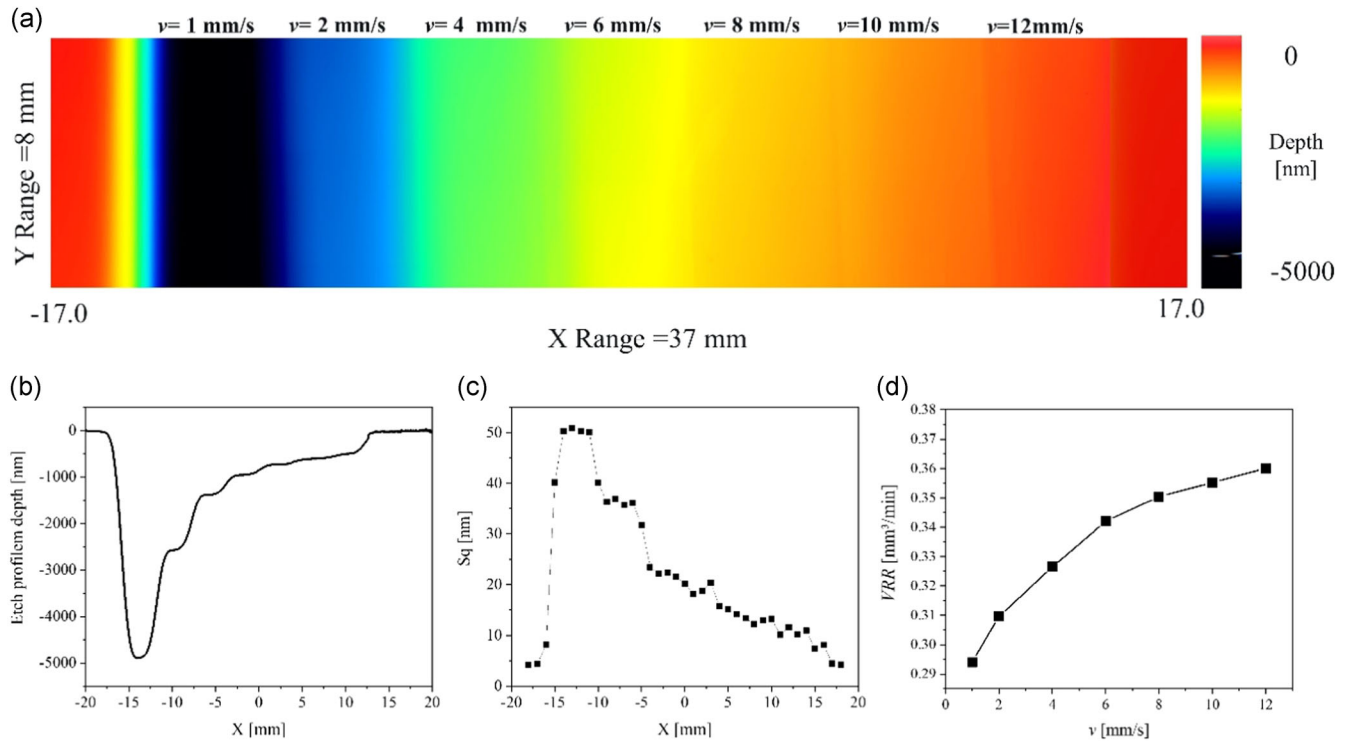

FIGURE 11 (a) Experimental area etching results, (b) cross-sectional shape of area, (c) surface roughness of N-BK7, (d) VRR of N-BK7 when the plasma jet moves over the surface from left to right, with an increasing value of velocity v from 1 to 12 mm/s at an initial temperature $T_h = 350°C$

4 | CONCLUSION

In this paper, fluorine-based PJM was applied for ultra-precise surface machining of N-BK7, aiming to clarify the underlying mechanisms of material removal, layer formation, and surface roughness evolution on N-BK7 surfaces at different surface temperatures. Moreover, the results for fused silica were presented in the assessment framework for comparison, as surface machining of fused silica by plasma jet is already well established. In the case of fused silica, local material removal on the substrate is realized by reactions of a CF_4 plasma discharge with fused silica (SiO_2), forming exclusively volatile etching products SiF_4 and CO_2. However, in the case of N-BK7, plasma-generated particles react with the surface and create nonvolatile compounds, in addition to volatile components. The nonvolatile compounds form a residual layer in the etched area, imposing unpredictable effects on the etching rate.

Our investigation showed that the thick residual layer noticeably degrades the capability of acquiring a targeted surface profile on N-BK7. However, the outcomes of this study reveal that the characteristics of residual layer during the machining process can be widely modified by adjusting the surface temperature T_s. In fact, surface temperature T_s is a significant factor that affects not only the etching rate of N-BK7 but also the features of the formed residual layer in the etching zone such as thickness and structure. To evaluate the effects of substrate temperature on the etching mechanism, the substrate was heated by a hot plate to an initial temperature T_h. The final value of the local surface temperature T_s was obtained by the sum of the plasma heat flow and an initial temperature T_h. It was shown that whenever the surface is adequately preheated at an initial temperature $T_h = 350°C$, a predictable static etching is achieved with a near-Gaussian shape profile depth, even at large values of dwell time. Since dynamic etching is a prerequisite for a deterministic dwell time-based machining scheme, an initial temperature $T_h = 350°C$ was chosen to perform a dynamic process on N-BK7 at different scan velocities v to assess the predictability of the etching profile for different plasma dwell times (or equivalently the velocity v of the plasma jet). It is concluded that at an initial temperature $T_h = 350°C$, a uniformly etched area with a predictable depth is achieved, even though a deep surface machining is performed. However, the VRR decreases and the surface roughness increases by reducing the scan velocity v.

ACKNOWLEDGMENT

The authors would like to thank D. Hirsch, Dr. J. Bauer and T. Liebeskind for supplying the measurement system. Financial support by German Federal Ministry of Education and Research (BMBF) within the framework of the InnoProfile-Transfer initiative 03IPT706X "Ultra-precision manufacturing using atomic particle beams" is gratefully acknowledged.

ORCID

Faezeh Kazemi http://orcid.org/0000-0003-2974-0726

REFERENCES

[1] H. Takino, N. Shibata, H. Itoh, T. Kobayashi, H. Tanaka, M. Ebi, K. Yamamura, Y. Sano, Y. Mori, *Appl. Opt.* **1998**, *37*, 5198.
[2] H. Takino, N. Shibata, T. Kobayashi, H. Itoh, H. Tanaka, A. Koike, K. Nakano, K. Yamamura, Y. Sano, Y. Mori, presented at Proc. 9th Intl. Conf. Product. Eng., Osaka, Japan, August–September 1999.
[3] T. Arnold, G. Boehm, A. Schindler, *J. Vac. Sci. Technol.* **2001**, *A 19*, 2586.
[4] T. Arnold, G. Boehm, H. Paetzelt, *Contrib. Plasma Phys.* **2014**, *54*, 145.
[5] T. Arnold, G. Boehm, H. Paetzelt, *J. Eur. Opt. Soc.-Rapid* **2016**, *11*, 16002.
[6] H. Paetzelt, G. Boehm, T. Arnold, *Plasma Sources Sci. Technol.* **2015**, *24*, 025002.
[7] M. Castelli, R. Jourdain, P. Morantz, P. Shore, *Precis. Eng.* **2012**, *36*, 467.
[8] Z. Dai, X. Xie, H. Chen, L. Zhou, *Plasma Chem. Plasma Process.* **2018**, *38*, 443.
[9] F. Kazemi, G. Boehm, T. Arnold, *Plasma Processes Polym.* **2019**, *16*, 12.
[10] F. Kazemi, G. Boehm, T. Arnold, presented at Optics Meas. 2019 Intl. Conf., Liberec, Czech Republic, October 2019.
[11] C. Constantine, *Micromach. Dev.* **1997**, *12*, 2.
[12] P. W. Leech, *Vacuum* **1999**, *55*, 191.
[13] H. Kreilkamp, *Analyse der Einflüsse auf die Gestaltabweichung gepresster Glasoptiken beim nicht-isothermen Blankpressen*, Apprimus Verlag, Aachen, Deutschland **2018**.
[14] G. Wang, H. Wang, L. Shen, J. Hou, Q. Xu, J. Wang, X. Chen, Z. Liu, *Appl. Opt.* **2018**, *57*, 2032.
[15] J. Meister, T. Arnold, *Plasma Chem. Plasma Process.* **2010**, *31*, 91.

How to cite this article: Kazemi F, Boehm G, Arnold T. An investigation on effectiveness of temperature treatment for fluorine-based reactive plasma jet machining of N-BK7®. *Plasma Process Polym*. 2020;17:e2000016.
https://doi.org/10.1002/ppap.202000016